

Constraint Learning for Parametric Point Cloud

Xi Cheng Ruiqi Lei Di Huang Zhichao Liao Fengyuan Piao Yan Chen
Pingfa Feng Long Zeng[†]

Tsinghua Shenzhen International Graduate School, Tsinghua University, Shenzhen, China

{chengxi23, leirq22}@mails.tsinghua.edu.cn, dihuangdylan@gmail.com,
{liaozc23, pfy22, chenyan23}@mails.tsinghua.edu.cn,
fengpff@tsinghua.edu.cn, zenglong@sz.tsinghua.edu.cn

Abstract

Parametric point clouds are sampled from CAD shapes, have become increasingly prevalent in industrial manufacturing. However, most existing point cloud learning methods focus on the geometric features, such as local and global features or developing efficient convolution operations, overlooking the important attribute of constraints inherent in CAD shapes, which limits these methods' ability to fully comprehend CAD shapes. To address this issue, we analyzed the effect of constraints, and proposed its deep learning-friendly representation, after that, the Constraint Feature Learning Network (CstNet) is developed to extract and leverage constraints. Our CstNet includes two stages. The Stage 1 extracts constraints from B-Rep data or point cloud. The Stage 2 leverages coordinates and constraints to enhance the comprehend of CAD shapes. Additionally, we built up the Parametric 20,000 Multi-modal Dataset for the scarcity of labeled B-Rep datasets. Experiments demonstrate that our CstNet achieved state-of-the-art performance on both public and proposed CAD shapes datasets. To the best of our knowledge, CstNet is the first constraint-based learning method tailored for CAD shapes analysis.

1. Introduction

Parametric point clouds are derived from parametric templates, which consist of primitives, constraints, and dimensional parameters. By specifying all parameters, the templates can be instantiated into CAD shapes, as illustrated in Figure 1. Parametric point clouds provide detailed information that is essential for various engineering applications, such as model design and product machining.

In recent years, deep learning methods have emerged as powerful tools for point cloud analysis, with models

such as PointNet [32], PointNet++ [33], and PointCNN [24] demonstrating significant success across various tasks. These models are primarily designed and evaluated on graphic objects, such as animals, trees, and other free-form shapes, where shape comprehension relies on geometric features visible in contours. However, some CAD shapes, despite exhibiting minimal visual differences, serve distinct purposes due to variations in their functional regions. This similarity in appearance poses challenge in distinguishing them based on geometric features. Notably, variations in the functional regions often introduce differing constraints, as these regions need to fit closely with other parts to perform functions such as transmission and positioning. Thus, distinguishing them from constraints-based perspective becomes more feasible, as illustrated in Figure 1.

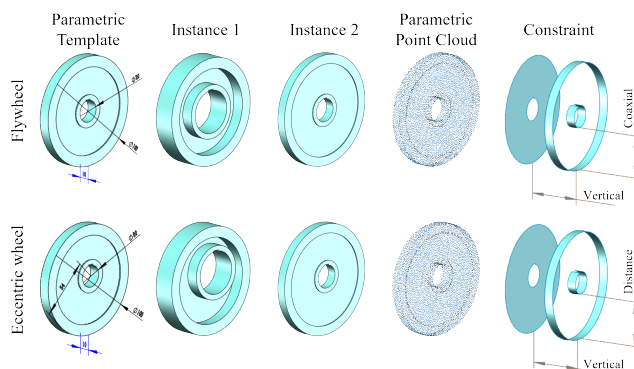


Figure 1. **Motivation.** Some similar CAD shapes serve different functions. The eccentric wheel has a rotation axis that is offset from its outer cylindrical surface, facilitating precise positioning or tension adjustment. In contrast, the flywheel has a coaxial rotation axis with its outer cylindrical surface and is used to store rotational kinetic energy. Although these shapes are challenging to distinguish visually, they can be easily differentiated from the perspective of constraints.

Additionally, the limited availability of B-Rep datasets poses barrier to deep learning on CAD shapes. Most ex-

Project page: <https://cstnetwork.github.io/>

isting CAD shapes datasets consist of mesh files, such as MCB [16] and ESB [12]. While mesh files could approximate the appearance of CAD shapes, lack crucial boundary information. In contrast, B-Rep data serves as the native representation of CAD shapes and is therefore more suitable for datasets construction. However, labeled B-Rep datasets remain relatively scarce, for example, FabWave [1] includes only 2,133 B-Rep files. Although the ABC [18] contains a large number of B-Rep files, it remains unlabeled.

To facilitate the constraint feature learning of CAD shapes, we conducted studies on deep learning methods and dataset development. Traditional constraint definitions are not well-suited for deep learning, as they vary across constraint types and involve multiple possible combinations to represent primitives' relation. To address this challenge, we proposed a novel constraint representation as point-wise local attributes. Afterwards, we developed the CstNet for constraint extraction and feature learning, which consist of two stages. The stage 1 is built for constraint acquisition, if B-Rep data is available, the openCASCADE Technology (OCCT) is used to extract constraints, otherwise the constraint prediction from point cloud (CST-PCD) module is adopted. The CST-PCD is designed relies on local features only, enabling it to generalize to unseen datasets after pre-training. The stage 2 leverages both point cloud and constraints for constraint feature learning, which employs both point-level and feature-level attention for effective feature extraction, enhancing the comprehension of CAD shapes. Finally, we built up a multi-modal classification dataset Parametric 20000, which contains B-Rep, Mesh, and point cloud. Given the current scarcity of labeled CAD shapes datasets, Parametric 20000 offers researchers an expanded resource for their work. Our contributions are threefold:

- We introduce the deep learning friendly expression of constraints.
- We designed the CstNet for constraint extraction and parametric feature learning.
- We collected and curated the Parametric 20000 dataset, which consist of mesh, point cloud, and B-Rep data.

Our CstNet has been validated across various tasks, on the mechanical classification dataset MCB [16], our model achieved an overall accuracy improvement of 2.98 % compared to the state-of-the-art, and for mechanical segmentation dataset 360 Gallery [19], that is 6.74 %.

2. Related Work

For the published deep learning methods focus on CAD shape are very few, and even fewer aimed at parametric point cloud, this section will provide an overview of existing point cloud learning methods as well as CAD shapes oriented models. By integrating insights from above areas, a comprehensive review of the relevant works could be presented.

2.1. Deep learning on point clouds

Point cloud deep learning can be categorized into three types based on data processing approaches: view-based, voxel-based, and point-based methods.

View-based methods typically project the point cloud from multiple views, the obtained figures are then fed in convolutional neural networks (CNNs) for feature extraction [6, 15, 37, 42, 53, 54]. However, these methods face significant challenges when applied to large-scale scanned data, primarily due to the difficulty of covering entire scenes from single-point perspectives, and the choice of projection views significantly impacts recognition performance. Besides that, it cannot be extended to 3D data segmentation or reconstruction easily.

Voxelization-based methods convert point cloud into 3D voxels, and then processed by 3D CNNs for feature extraction [17, 20, 30, 35, 40, 47]. However, the size and orientation of the voxels can affect computational efficiency, memory usage. The voxel grid quantization process may lead to geometric detail lost, and the inherent sparsity of point clouds may result in many useless voxels.

Point-based methods directly use points as input, thereby avoiding information loss associated with view-based and voxel-based methods, it is also the most popular point cloud learning method [2, 4, 7, 9, 10, 24, 26–28, 32–34, 38, 41, 46, 48–50, 52, 55, 56]. Typically, symmetric functions and k-nearest neighbors (KNN) are employed for feature extraction. However, the unordered nature and transformation invariance of point clouds pose challenges for efficient feature extraction.

2.2. Deep learning on CAD shapes

CAD shapes deep learning can be categorized into three types based on the input data format: B-Rep-based learning, mesh-based learning, and sketch-based learning.

B-Rep-based methods typically involve B-Rep data conversion and feature extraction. Since B-Rep data cannot be directly fed into deep learning models, the challenge lies in converting B-Rep into deep learning compatible format, with graph representation is commonly used. These approaches are commonly applied to classification [13], segmentation [5, 19], assembly [14, 43], engineering sketch generation [11], and CAD operation sequence prediction [45, 57].

Mesh-based learning methods use triangle models as input, such as STL and OBJ. Compared to B-Rep, mesh representations lack boundary details, which prevents these methods from leveraging data conversion for improved performance. As a result, contributions often rely on mechanical datasets provided by the authors. These methods are primarily used for classification [29], retrieval [3], segmentation [39], and B-Rep generation [8].

Sketch-based learning takes hand-drawn sketches as input, with outputs typically being engineering sketches [8, 25, 31, 36, 44], 3D models [21, 22], or CAD operation sequences [51]. Most of these models are generative, and utilizing transformer modules frequently. A key challenge is incorporating the regularity and connectivity of primitives, which typically overlooked in graphic objects analysis.

While there has been substantial progress in above domains, the engineering applications of parametric point cloud analysis demand further innovation to ensure accuracy and robustness.

3. Method

3.1. Problem Statement

Constraints is crucial for CAD shapes, can they be utilized to enhance deep learning methods' performance? To answer above question, we designed the following experiments. The objective is to compare the prisms shown in Figure 2 with cuboids. In each experiment, only prisms with a specific angle are selected, creating a binary classification task between prisms and cuboids. Consequently, eight independent experiments are conducted to cover all angles. As the prism's angle approaches 90°, its resemblance to cuboids increases, making it progressively more challenging to distinguish them. The constraint-aware model is built on PointNet++ backbone, which predict constraints and then adopt it for classification, more details in supplementary.

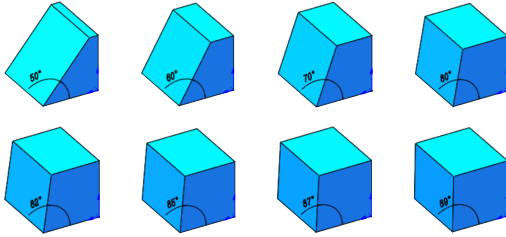


Figure 2. Prisms compared to cuboid.

The experimental results are presented in Figure 3. For prisms with angle of 50° and 89°, the constraints have little improvement on the results. The reason lies in the 50° prism differs substantially from the cuboid, while the 89° prism is too similar to the cuboid. For other circumstances, incorporating constraints improves classification accuracy significantly, demonstrating that the constraint enhanced model's comprehension on CAD shapes.

However, the constraint learning method designed in the validation experiments is only applicable to simple scenarios. To develop a more generalized approach, we further investigated the constraint representation and deep learning architecture tailored for parametric point clouds.

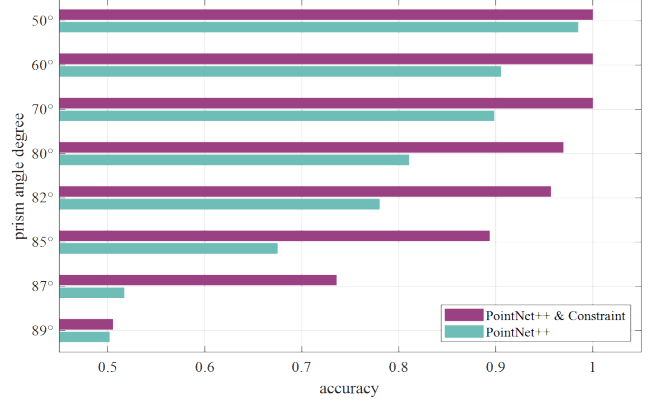


Figure 3. Classification accuracy of validation experiments.

3.2. Constraint Representation

Constraint should be defined as point-wise attribute for point cloud, analogous to normal vector, as point cloud is inherently unordered, assigning constraints at the point-wise level ensures that their representation is independent of point permutation.

Following the constraint definition in CAD software is not applicable, However, once constraint is applied, the positional relations between primitives become fixed. Therefore, if the type of primitives and their relations are determined, the constraint on CAD shape can be defined comprehensively.

The point-wise primitive type could be represented as the type of the primitive which the point aligned to, using one-hot encoding.

The positional relation is defined as the combination of main axis direction and adjacency. Considering that the direction of primitives' main axis is unique, as shown in Figure 4, relations such as parallel and vertical could be derived by the direction of their main axes. However, some dimensional relations can not, such as the cylinders' radius equivalence. Thus, additional data is required to supplement this information.

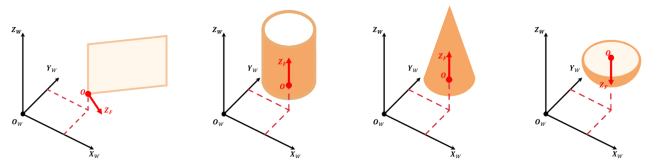


Figure 4. Main axis of primitives. Plane: normal vector. Cylinder, cone, and sphere: rotation axis.

Since the connected primitives are the basis of CAD shapes, the adjacency and main axis direction impose limitation on the distance and size of other primitives. For example, in a cuboid, the adjacency and normal of the six faces ensures that the distance between the top and bottom

faces equals the height of the front face, and the size of the back face is the same as the front one. Therefore, if the adjacency combined with main axis directions, the positional relation can be determined comprehensively.

Adjacency represents the connection between primitives and cannot be expressed as point-wise attribute directly. The edges are the key indicator of adjacency, with each edge corresponding to two adjacent primitives, adjacency can therefore be inferred from edges. For point cloud, an edge can be represented by marking points near it, thus, point-wise adjacency is expressed as whether the point is near an edge, which can be represented by two-channel one-hot vector.

In summary, each composition of constraints in parametric point cloud is illustrated in Figure 5, and each point with constraint is expressed as (Coordinate, Primitive Type, Main Axis Direction, Adjacency).

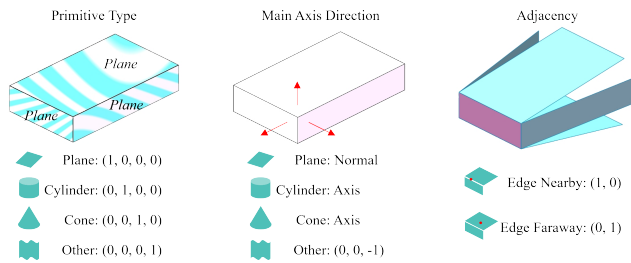


Figure 5. Constraint representation of parametric point cloud.

3.3. Method Overview

Our CstNet and module details are depicted in the top and bottom side of Figure 6 respectively. It should be noted that the CST-PCD module requires pre-training, and once the pre-training is completed, its parameters are kept frozen. Given the locality of the constraints expression we designed, the pre-trained CST-PCD module is able to generalize to other unseen mechanical datasets directly. In this work, the dataset for pre-training CST-PCD module comes from ABC [18].

3.4. Constraint Acquisition

When B-Rep data is available, the CST-BRep module can be used to compute constraints.

For the input B-Rep data, tessellation is performed by OCCT to generate a mesh model, followed by Poisson disk sampling [23] via pymeshlab to ensure a uniform point distribution and control the point count, if point cloud generation is not needed, this step could be skipped.

For adjacency computation, we identify valid edges firstly. In this study, an edge is considered invalid if the two adjacent faces are smoothly connected along the edge, this work is accomplished by OCCT. Next, we compute the distance from each point to all valid edges. A point

is marked as near an edge if the minimum distance is below a threshold (determined by the model surface area, set to $0.08 \times Area/4\pi$ in this paper). For the primitive type and main axis direction of a point, we first determine which face it aligned with, OCCT is then used to analyze the face, providing both the face type and main axis direction.

In the absence of B-Rep data, such as working with mesh or voxel models, it can be converted into point cloud, after which the CST-PCD module can be used to predict constraints. Since each point’s constraints are local information, the computation only requires data from its neighboring points, meaning that global information is unnecessary. The constraint computation of a point p could be divided into the following steps:

Step 1. Identify neighbor points around p .

Step 2. From all neighbor points, identify which belong to the same primitive as p , these points are referred to as valid points.

Step 3. Fit shapes such as cylinders or planes using the valid points, and determine the primitive type with the smallest fitting error.

Step 4. Based on the the valid points and the primitive type, calculate the main axis direction and assess whether the point is near an edge.

While the above process can be carried out using traditional methods, it is highly complex, which is why a deep learning model is employed to achieve the same.

The design of CST-PCD module is inspired by the aforementioned calculation process. For **Step 1**, which involves finding neighbor points, the traditional approach is to use the K Nearest Neighbors (KNN) algorithm, which identifies neighbors within a sphere. However, for constraint computation, it is more effective to search for neighbors along the shape’s surface. This approach captures more relevant points while reducing the influence of redundant points, as shown in Figure 7. To this end, we proposed a neighbor searching method called SurfaceKNN, details in supplementary.

For **Step 2**, which involves identifying valid points from neighbors, the attention mechanism between points is employed to approximate this process, which applying different weight to neighbor points when updating the center point’s embedding. We designed the point attention layer based on vector self-attention, the relation between points is designed as embedding subtraction, as shown in Equation (1).

$$\mathbf{f}'_i = \sum_{f_j \in \mathcal{N}_i} \rho(\text{mlp}(Q(\mathbf{f}_i) - K(\mathbf{f}_j))) \odot V(\mathbf{f}_i). \quad (1)$$

Where \mathcal{N}_i is the feature collection of all neighbor points around p_i , ρ is the normalization function (softmax in this paper), and \odot denotes element-wise multiplication. $Q(\mathbf{f})$,

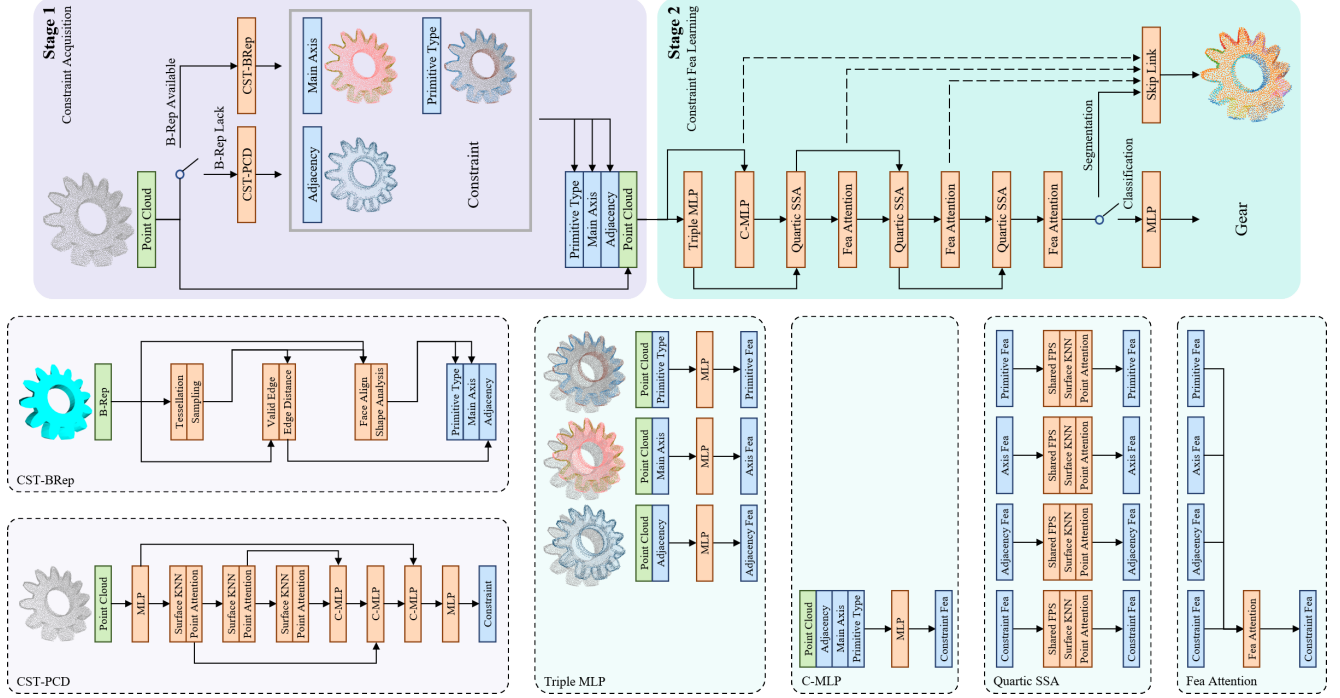


Figure 6. **Overview of CstNet.** The top side illustrates the overall architecture of CstNet, comprising two stages. Stage 1 is designed for constraint acquisition. When B-Rep data is available, the CST-BRep module is utilized to extract constraints; otherwise, use the CST-PCD predicts constraints. Stage 2 perform constraint feature learning, facilitate deeper understanding for CAD shapes. The bottom side presents the details of module design.

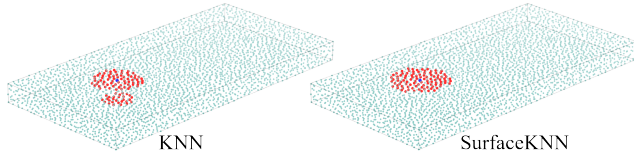


Figure 7. **Comparison of KNN and SurfaceKNN.** Blue point: center, red point: neighbor.

$K(\mathbf{f})$, and $V(\mathbf{f})$ are defined in the same way by concatenating \mathbf{f} with the positional encoding Δ and then feeding it into MLP, where Δ is defined as $\Delta = \mathbf{p}_i - \mathbf{p}_j$.

Step 3 and **Step 4** involve determining the Primitive Type and Main Axis Direction, both steps can be accomplished by MLPs. We employed a U-Net-like structure to enhance information utilization. In the CST-PCD module, C-MLP refers to concatenating the input tensors and feeding them into MLPs. The final MLP in this module consists of three parallel MLPs with the same input, where the outputs correspond to Primitive Type, Main Axis Direction, and Adjacency.

The structure of CST-PCD module reveals that only local information is utilized, which aligns with the inherently local nature of the constraint representation we designed. For no global information is incorporated and most CAD

shapes consist of a limited set of local geometry, such as plane, cylinder, and sphere, the CST-PCD can generalize to unseen datasets if pre-trained on a large dataset. As a result, our CST-PCD enables the effective use of existing unlabeled B-Rep datasets, making it possible to serve for meaningful tasks.

3.5. Constraint Feature Learning

The stage 2 of CstNet is designed to leverage constraints to deepen the model’s understanding of CAD shapes. The designed architecture extract features from Primitive Type, Main Axis Direction, and Adjacency separately, attention between features is then applied to update constraint feature. The structure and module details are illustrated in Figure 6.

The Triple MLP takes the point cloud, Primitive Type, Main Axis Direction, and Adjacency as inputs. In this module, the point cloud is concatenated with the Primitive Type, Main Axis Direction, and Adjacency separately before being fed into three individual MLPs. The outputs are the Primitive Feature, Axis Feature, and Adjacency Feature, respectively.

In the C-MLP layer, point cloud is concatenated with Primitive Type, Main Axis Direction, Adjacency, and then feed into MLP, with the output being the Parametric Fea-

ture.

The Quartic SSA layer takes the Primitive Feature, Axis Feature, Adjacency Feature, and Parametric Feature as input. This layer consists of four paths, each processing the corresponding feature independently. In each path, Farthest Point Sampling (FPS) is performed to reduce the point scale. Subsequently, SurfaceKNN is used to search neighbors of each sampled point. The output of FPS and SurfaceKNN are shared across the four paths. Finally, point attention is employed for updating sampled points' feature by its neighbors, with a slight modification in the positional encoding Δ of Equation (1). For the path takes XYZ & Main Axis Direction as input, $\Delta = [(\mathbf{p}_i - \mathbf{p}_j) \parallel (\mathbf{n}_i - \mathbf{n}_j)]$, \mathbf{n}_i represents the main axis direction of \mathbf{p}_i . For the paths that use XYZ & Primitive Type or Adjacency as input, $\Delta = [(\mathbf{p}_i - \mathbf{p}_j) \parallel \mathbf{a}_i \parallel \mathbf{a}_j]$, where \mathbf{a}_i is the one-hot encoding of Primitive Type or Adjacency, $[\cdot \parallel \cdot]$ indicates concatenation in feature channel. Through sampling, neighbor searching, and attention, the point cloud is down-scaled and features are updated.

The Fea Attention layer also takes the Primitive Feature, Axis Feature, Adjacency Feature, and Parametric Feature as input, attention between features is employed to update constraint feature efficiently. This design is considered that different points may focus on different features, for example, points near edge may focus more on the Adjacency Feature, while others may pay more attention to the Primitive or Axis Feature. The Fea Attention is developed by vector attention as formulated in Equation (2).

$$\mathbf{f}'_{cst} = \sum_{\mathbf{f}_j \in \mathcal{F}} \rho \left(\text{mlp}(\mathbf{Q}(\mathbf{f}_{cst}) - \mathbf{K}(\mathbf{f}_j)) \right) \odot \mathbf{V}(\mathbf{f}_{cst}). \quad (2)$$

In which $\mathcal{F} = \{\mathbf{f}_{pmt}, \mathbf{f}_{axs}, \mathbf{f}_{adj}, \mathbf{f}_{cst}\}$, \mathbf{f}_{pmt} is Primitive Feature, \mathbf{f}_{axs} is Axis Feature, \mathbf{f}_{adj} is Adjacency Feature, and \mathbf{f}_{cst} is Constraint Feature. Δ is defined as one-hot encoding of \mathbf{f}_j type.

For downstream tasks, if classification is required, the final constraint feature can be fed into MLP and softmax. For segmentation tasks, upsampling and skip link concatenation similar to those in PointNet++ [33] can be applied.

4. Experiments

4.1. Experimental Settings

In general, we train CstNet using the Negative Log Likelihood Loss (NLLLoss) and optimized by Adam optimization for 200 epochs, with a weight decay of 0.0001 and an initial learning rate of 0.0001. We use StepLR learning rate scheduler, with step size of 20 and gamma of 0.7. The batch size is 16. All experiments are performed on GeForce RTX 4090 GPU.

Parametric 20000 dataset: our Parametric 20000 dataset contains 19,739 multi-modal instances categorized into 75 classes. Each instance includes B-Rep data, mesh, and point cloud. All B-Rep data are collected from the following three sources. More details in the supplementary.

Sources 1 (36.05 %): Downloaded and purified from TraceParts [16]. The CAD shapes on TraceParts are collected from manufacturing companies.

Sources 2 (24.12 %): Provided by a CAD company¹ that collaborates with our team. These shapes are all mechanical components.

Sources 3 (39.83 %): Instantiated from parametric templates designed by our team. These templates are designed based on common mechanical structures.

Our Parametric 20000 dataset encompasses various common formats of CAD shapes, making it suitable for a wide range of tasks. The careful selection and purification process undertaken by our team further ensures its high quality.

4.2. Constraint Acquisition

The extraction of constraints from B-Rep data is accomplished by CST-BRep module, with results visualized in the "GT" column of Figure 8. By referring the model row, this module performs well in extracting three components of constraint.

Extract constraints from point cloud is achieved by CST-PCD module. The training set is sourced from 25 Trunks of ABC [18], with each trunk containing 10,000 B-Rep files. We utilized CST-BRep to extract constraints as Ground Truth for model training. After the training finished, the prediction accuracy of Primitive Type reached 94.23 %, for Adjacency, that is 94.62 %, and the MSE loss for Main Axis Direction is 0.0559.

In subsequent classification and segmentation tasks, above pre-trained CST-PCD module is utilized to predict constraints with its weights frozen and no further updates. To ensure that only point cloud is used as input across all methods in comparison, even when B-Rep data is available, the CST-BRep module will not be activated to obtain constraints.

After CST-PCD module is pre-trained, we evaluated it on a new Trunk of ABC. The visualization of constraint prediction is shown in the "Pred." column of Figure 8. After traversing this Trunk, the prediction accuracy of Primitive Type reached 91.19 %, for Adjacency, that is 90.24 %, the MSE loss of Main Axis Direction is 0.0998, above demonstrating the strong capability for constraint prediction.

Additionally, we evaluated the pre-trained CST-PCD module on the CAD shapes dataset MCB [16] to predict constraints. For the MCB consists of mesh files, it was not possible to extract ground truth constraints for comparison. Based on the results visualized in Figure 9, CST-PCD

¹<https://www.newdimchina.com/>

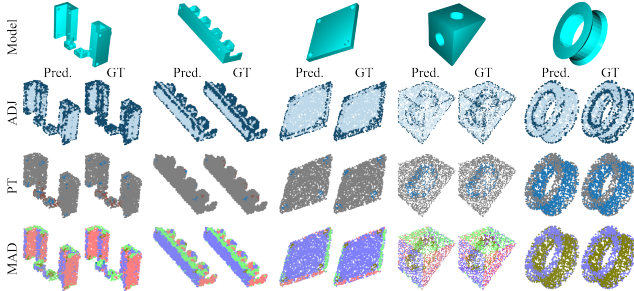


Figure 8. **Constraint prediction on ABC.** MAD: Main Axis Direction. PT: Primitive Type. ADJ: Adjacency (whether point is near edge). Main Axis Direction has been processed for visualization, details in supplementary.

Table 1. **Classification results on Parametric 20000.** Acc: accuracy over instance %, Acc*: accuracy over class %, F1: F1-score, mAP: mean average precision %.

Method	Acc	Acc*	F1	mAP
PointCNN [24]	61.92	55.29	53.97	40.99
PointNet [32]	75.61	74.08	74.23	82.15
PointNet++ [33]	82.89	86.80	82.31	88.05
PointConv [46]	80.53	82.10	81.86	86.54
DGCNN [41]	85.99	88.20	87.20	89.20
3DGCN [26]	86.19	86.31	85.37	87.64
Ours	89.93	91.04	90.32	92.32

demonstrated a high level of constraint prediction accuracy even on an unseen dataset.

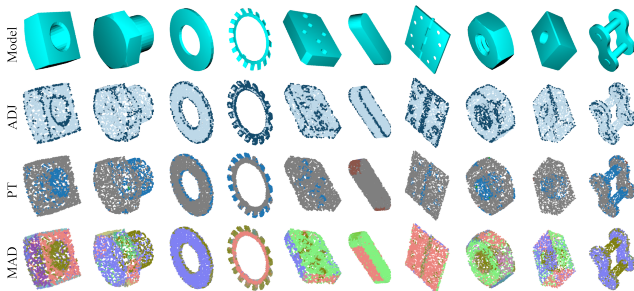


Figure 9. **Constraint prediction on MCB.**

4.3. Classification

The classification results on the Parametric 20000 dataset are presented in Table 1, where our CstNet outperformed other methods across both metrics. Additionally, the instance accuracy of all methods is below 90 %, with a notable performance gap between them, indicating that this dataset poses challenges and effectively differentiates between methods.

We conducted evaluations on the CAD shapes dataset

MCB [16], with results presented in Table 2. Our CstNet achieved the highest scores across all metrics on MCB-A, but performed less effectively on MCB-B. This discrepancy may stem from the composition of MCB: MCB-A includes shapes from TraceParts (69.27 %), 3D Warehouse (21.70 %), and GrabCAD (9.03 %), while MCB-B is limited to shapes from 3D Warehouse and GrabCAD. TraceParts provides data from manufacturing companies, whereas 3D Warehouse and GrabCAD contain shapes for general usages [16]. As the CST-PCD module in CstNet is pre-trained on ABC, which primarily comprises mechanical components, this pre-training may lead to poor constraint prediction performance on MCB-B, thereby influencing the classification results.

4.4. Segmentation

We conducted experiments on the mechanical segmentation dataset 360 Gallery [19], which contains point clouds with segmentation labels based on CAD modeling operations. However, this labeling approach presents disadvantage for point cloud segmentation. For example, a cube in this dataset has four faces labeled as "ExtrudeSide" and two faces labeled as "ExtrudeEnd", which poses an unrealistic task for point cloud networks. Additionally, the distribution of points across different labels is highly imbalanced. For instance, points labeled as "ExtrudeSide" accounts for 45.94 %, while those labeled as "RevolveEnd" make up only 0.12 %. Despite these limitations, to our knowledge, 360 Gallery is currently the only publicly available point cloud dataset for CAD shapes segmentation task.

The segmentation results are presented in Table 3, where our method outperforms the state-of-the-art methods on most metrics. The results also highlight the limitations of this 360 Gallery in terms of point cloud segmentation. Apart from "ExtrudeSide" and "ExtrudeEnd", none of the models were able to differentiate the other segmentation categories except DGCNN managed to predict "RevolveSide" with a low mIoU.

A portion of the segmentation results on 360 Gallery test set are shown in Table 4, where our CstNet shows segmentation results closest to the Ground Truth. PointNet's segmentation differs from other methods, for instance, in the third and fourth rows, PointNet mistakenly segments a single primitive into two different categories. This discrepancy likely arises from the model's inability to effectively capture local features.

4.5. Ablation Studies

Our model leverages all three components of constraint: Primitive Type, Main Axis Direction, and Adjacency. Additionally, we utilized the SurfaceKNN to obtain more suitable neighbors for each point. To validate the effectiveness of our design, we conducted a series of experiments

Table 2. **Classification results on MCB.** A / B column: results of MCB A / B subset.

Method	Acc.instance %		Acc.class %		F1-score		mAP %	
	A	B	A	B	A	B	A	B
PointCNN [24]	93.89	93.67	81.85	86.80	83.86	88.63	90.13	93.86
PointNet [32]	86.78	80.36	67.70	65.30	86.55	79.89	74.08	71.66
PointNet++ [33]	87.45	93.91	73.68	87.97	88.32	73.45	91.33	91.37
SpiderCNN [52]	93.59	89.31	79.70	79.29	81.30	80.72	86.64	82.47
PointConv [46]	93.25	90.64	80.24	80.17	71.31	76.07	82.19	86.09
DGCNN [41]	92.54	90.75	74.47	78.17	76.12	79.69	74.27	79.73
3DGCN [26]	93.71	92.13	78.71	84.31	84.59	79.24	84.35	84.35
Ours	96.87	92.61	89.21	85.94	89.85	85.68	93.17	91.25

Table 3. **Part Segmentation Results on 360 Gallery.** PN: PointNet. PN2: PointNet++. DGN: DGCNN. 3DN: 3DGCN. OA: overall accuracy %. mIoU: instance mIoU. mIoU*: class mIoU. ESide: extrude side mIoU, EEnd: extrude end mIoU. Other segmentation categories' mIoU are all 0 except RevolveSide mIoU of DGCNN is 9.60, more details in supplementary.

Method	OA	mIoU	mIoU*	ESide	EEnd
PN [32]	42.13	18.89	7.04	19.83	36.47
PN2 [33]	58.18	26.98	11.27	49.80	40.36
DGN [41]	64.02	35.54	14.36	54.48	50.82
3DN [26]	60.58	33.03	12.23	50.67	47.20
Ours	70.76	46.65	20.51	61.29	60.65

Table 4. **Visualization of part segmentation on 360 Gallery.** GT: ground truth. PN: PointNet [32]. PN2: PointNet++ [33]. DGN: DGCNN [41]. 3DN: 3DGCN [26].

GT	PN	PN2	DGN	3DN	Ours

on Parametric 20000 dataset.

For each component of constraint, we evaluated their importance by disable one at a time. This operation is conducted by setting it as a zero tensor before feeding into the

Table 5. **Effects on Parametric 20000 dataset with varying neighbor search and constraints.** Row 3 - 6: SurfaceKNN, Row 7 - 10: KNN.

Constraint			Acc	Acc*	F1	mAP
MAD	ADJ	PT				
✓	✓	✓	89.93	91.04	90.32	92.32
✗	✓	✓	86.32	89.05	88.38	90.59
✓	✗	✓	88.14	89.61	88.64	91.35
✓	✓	✗	88.68	88.94	89.01	91.22
✓	✓	✓	89.03	90.00	89.22	91.43
✗	✓	✓	85.04	85.93	85.74	88.08
✓	✗	✓	87.27	88.23	87.98	90.00
✓	✓	✗	88.73	88.97	88.91	91.21

model. The results are presented in Table 5, which show that all three components contribute to improve the performance of our CstNet.

To assess the effectiveness of SurfaceKNN, we compared it with KNN. From Table 5, it can be concluded that in most cases, our SurfaceKNN outperforms KNN. However, when Primitive Type is disabled, the results are similar between the two methods, indicating that SurfaceKNN primarily enhances the effectiveness of the Primitive Feature.

5. Conclusions

In this paper, we studied the CAD shapes and introduced the constraints expression which suitable for deep learning methods. Afterward, we proposed the CstNet for extracting and learning constraint features. Additionally, we built up a multimodal CAD shape classification dataset Parametric 20000. Experimental results on both public datasets and proposed dataset demonstrate that our CstNet achieves state-of-the-art performance across multiple metrics. Comprehensive ablation studies further validate that each component of constraint and SurfaceKNN contributes to im-

prove the performance of CstNet.

CAD shapes possess numerous attributes. In this paper, we analyze the constraints from functional perspective. In future work, we plan to investigate additional aspects such as part design and manufacturing processes, to achieve a deeper understanding of CAD shapes.

References

- [1] A. Angrish, B. Craver, and B. Starly. Fabsearch: A 3d cad model-based search engine for sourcing manufacturing services. *Journal of Computing and Information Science in Engineering*, 19(4), 2019. Export Date: 08 October 2024; Cited By: 23. [2](#)
- [2] M. Atzmon, H. Maron, and Y. Lipman. Point convolutional neural networks by extension operators. *ACM Transactions on Graphics*, 37(4), 2018. Export Date: 31 July 2024; Cited By: 222. [2](#)
- [3] D. Y. Chen, X. P. Tian, Y. T. Shen, and M. Ouhyoung. On visual similarity based 3d model retrieval. In *Computer Graphics Forum*, volume 22, pages 223–232, 2003. Export Date: 28 June 2024; Cited By: 1323. [2](#)
- [4] Yan Chen, Di Huang, Zhichao Liao, Xi Cheng, Xinghui Li, and Lone Zeng. Training-free point cloud recognition based on geometric and semantic information fusion. *arXiv preprint arXiv:2409.04760*, 2024. [2](#)
- [5] E. Dupont, K. Cherenkova, A. Kacem, S. A. Ali, I. Arzhankov, G. Gusev, and D. Aouada. Cadops-net: Jointly learning cad operation types and steps from boundary-representations. In *Proceedings - 2022 International Conference on 3D Vision, 3DV 2022*, pages 114–123, 2022. Export Date: 06 July 2024; Cited By: 2. [2](#)
- [6] Y. Feng, Z. Zhang, X. Zhao, R. Ji, and Y. Gao. Gvcnn: Group-view convolutional neural networks for 3d shape recognition. In *Proceedings of the IEEE Computer Society Conference on Computer Vision and Pattern Recognition*, pages 264–272, 2018. Export Date: 31 July 2024; Cited By: 502. [2](#)
- [7] A. Goyal, H. Law, B. Liu, A. Newell, and J. Deng. Revisiting point cloud shape classification with a simple and effective baseline. In *Proceedings of Machine Learning Research*, volume 139, pages 3809–3820, 2021. Export Date: 31 July 2024; Cited By: 92. [2](#)
- [8] H. Guo, S. Liu, H. Pan, Y. Liu, X. Tong, and B. Guo. Complexgen: Cad reconstruction by b-rep chain complex generation. *ACM Transactions on Graphics*, 41(4), 2022. Export Date: 23 July 2024; Cited By: 20. [2, 3](#)
- [9] M. H. Guo, J. X. Cai, Z. N. Liu, T. J. Mu, R. R. Martin, and S. M. Hu. Pct: Point cloud transformer. *Computational Visual Media*, 7(2):187–199, 2021. Export Date: 31 July 2024; Cited By: 917. [2](#)
- [10] Q. Huang, W. Wang, and U. Neumann. Recurrent slice networks for 3d segmentation of point clouds. In *Proceedings of the IEEE Computer Society Conference on Computer Vision and Pattern Recognition*, pages 2626–2635, 2018. Export Date: 31 July 2024; Cited By: 391. [2](#)
- [11] F. Hähnlein, C. Li, N. J. Mitra, and A. Bousseau. Cad2sketch. *ACM Transactions on Graphics*, 41(6), 2022. Export Date: 23 July 2024; Cited By: 1. [2](#)
- [12] S. Jayanti, Y. Kalyanaraman, N. Iyer, and K. Ramani. Developing an engineering shape benchmark for cad models. *CAD Computer Aided Design*, 38(9):939–953, 2006. Export Date: 08 October 2024; Cited By: 280. [2](#)
- [13] P. K. Jayaraman, A. Sanghi, J. G. Lambourne, K. D. D. Willis, T. Davies, H. Shayani, and N. Morris. Uv-net: Learning from boundary representations. In *Proceedings of the IEEE Computer Society Conference on Computer Vision and Pattern Recognition*, pages 11698–11707, 2021. Export Date: 28 June 2024; Cited By: 27. [2](#)
- [14] Benjamin Jones, Dalton Hildreth, Duowen Chen, Ilya Baran, Vladimir G. Kim, and Adriana Schulz. Automate: a dataset and learning approach for automatic mating of cad assemblies. *ACM Transactions on Graphics*, 40(6):1–18, Dec. 2021. [2](#)
- [15] E. Kalogerakis, M. Averkiou, S. Maji, and S. Chaudhuri. 3d shape segmentation with projective convolutional networks. In *Proceedings - 30th IEEE Conference on Computer Vision and Pattern Recognition, CVPR 2017*, volume 2017-January, pages 6630–6639, 2017. Export Date: 31 July 2024; Cited By: 256. [2](#)
- [16] S. Kim, H. G. Chi, X. Hu, Q. Huang, and K. Ramani. A large-scale annotated mechanical components benchmark for classification and retrieval tasks with deep neural networks. In *Lecture Notes in Computer Science (including subseries Lecture Notes in Artificial Intelligence and Lecture Notes in Bioinformatics)*, volume 12363 LNCS, pages 175–191, 2020. Export Date: 07 October 2024; Cited By: 33. [2, 6, 7](#)
- [17] R. Klokov and V. Lempitsky. Escape from cells: Deep kd-networks for the recognition of 3d point cloud models. In *Proceedings of the IEEE International Conference on Computer Vision*, volume 2017-October, pages 863–872, 2017. Export Date: 31 July 2024; Cited By: 857. [2](#)
- [18] S. Koch, A. Matveev, Z. Jiang, F. Williams, A. Artemov, E. Burnaev, M. Alexa, D. Zorin, and D. Panozzo. Abc: A big cad model dataset for geometric deep learning. In *Proceedings of the IEEE Computer Society Conference on Computer Vision and Pattern Recognition*, volume 2019-June, pages 9593–9603, 2019. Export Date: 08 October 2024; Cited By: 279. [2, 4, 6](#)
- [19] J. G. Lambourne, K. D. D. Willis, P. K. Jayaraman, A. Sanghi, P. Meltzer, and H. Shayani. Brepnet: A topological message passing system for solid models. In *Proceedings of the IEEE Computer Society Conference on Computer Vision and Pattern Recognition*, pages 12768–12777, 2021. Export Date: 28 June 2024; Cited By: 31. [2, 7](#)
- [20] T. Le and Y. Duan. Pointgrid: A deep network for 3d shape understanding. In *Proceedings of the IEEE Computer Society Conference on Computer Vision and Pattern Recognition*, pages 9204–9214, 2018. Export Date: 31 July 2024; Cited By: 324. [2](#)
- [21] C. Li, H. Pan, A. Bousseau, and N. J. Mitra. Sketch2cad: Sequential cad modeling by sketching in context. *ACM Transactions on Graphics*, 39(6), 2020. Export Date: 23 July 2024; Cited By: 42. [3](#)
- [22] C. Li, H. Pan, A. Bousseau, and N. J. Mitra. Free2cad: Parsing freehand drawings into cad commands. *ACM Transactions on Graphics*, 41(4), 2022. Export Date: 23 July 2024;

- Cited By: 27. 3
- [23] Hongwei Li. *Poisson disk sampling: modern techniques*. Thesis, The Hong Kong University of Science and Technology Library, 2010. 4
- [24] Y. Li, R. Bu, M. Sun, W. Wu, X. Di, and B. Chen. Pointcnn: Convolution on x-transformed points. In *Advances in Neural Information Processing Systems*, volume 2018-December, pages 820–830, 2018. Export Date: 08 October 2024; Cited By: 1859. 1, 2, 7, 8
- [25] Zhichao Liao, Di Huang, Heming Fang, Yue Ma, Fengyuan Piao, Xinghui Li, Long Zeng, and Pingfa Feng. Free-hand sketch generation from mechanical components. *arXiv preprint arXiv:2408.05966*, 2024. 3
- [26] Z. H. Lin, S. Y. Huang, and Y. C. F. Wang. Learning of 3d graph convolution networks for point cloud analysis. *IEEE Transactions on Pattern Analysis and Machine Intelligence*, 44(8):4212–4224, 2022. Export Date: 08 October 2024; Cited By: 35. 2, 7, 8
- [27] Y. Liu, B. Fan, S. Xiang, and C. Pan. Relation-shape convolutional neural network for point cloud analysis. In *Proceedings of the IEEE Computer Society Conference on Computer Vision and Pattern Recognition*, volume 2019-June, pages 8887–8896, 2019. Export Date: 31 July 2024; Cited By: 664.
- [28] X. Ma, C. Qin, H. You, H. Ran, and Y. Fu. Rethinking network design and local geometry in point cloud: A simple residual mlp framework. In *ICLR 2022 - 10th International Conference on Learning Representations*, 2022. Export Date: 31 July 2024; Cited By: 172. 2
- [29] B. Manda, P. Bhaskare, and R. Muthuganapathy. A convolutional neural network approach to the classification of engineering models. *IEEE Access*, 9:22711–22723, 2021. Export Date: 28 June 2024; Cited By: 18. 2
- [30] D. Maturana and S. Scherer. Voxnet: A 3d convolutional neural network for real-time object recognition. In *IEEE International Conference on Intelligent Robots and Systems*, volume 2015-December, pages 922–928, 2015. Export Date: 31 July 2024; Cited By: 2809. 2
- [31] W. R. Para, S. F. Bhat, P. Guerrero, T. Kelly, N. Mitra, L. Guibas, and P. Wonka. Sketchgen: Generating constrained cad sketches. In *Advances in Neural Information Processing Systems*, volume 7, pages 5077–5088, 2021. Export Date: 07 July 2024; Cited By: 23. 3
- [32] C. R. Qi, H. Su, K. Mo, and L. J. Guibas. Pointnet: Deep learning on point sets for 3d classification and segmentation. In *Proceedings - 30th IEEE Conference on Computer Vision and Pattern Recognition, CVPR 2017*, volume 2017-January, pages 77–85, 2017. Export Date: 31 July 2024; Cited By: 9040. 1, 2, 7, 8
- [33] C. R. Qi, L. Yi, H. Su, and L. J. Guibas. Pointnet++: Deep hierarchical feature learning on point sets in a metric space. In *Advances in Neural Information Processing Systems*, volume 2017-December, pages 5100–5109, 2017. Export Date: 31 July 2024; Cited By: 6263. 1, 6, 7, 8
- [34] S. Qiu, S. Anwar, and N. Barnes. Geometric back-projection network for point cloud classification. *IEEE Transactions on Multimedia*, 24:1943–1955, 2022. Export Date: 31 July 2024; Cited By: 110. 2
- [35] G. Riegler, A. O. Ulusoy, and A. Geiger. Octnet: Learning deep 3d representations at high resolutions. In *Proceedings - 30th IEEE Conference on Computer Vision and Pattern Recognition, CVPR 2017*, volume 2017-January, pages 6620–6629, 2017. Export Date: 31 July 2024; Cited By: 1052. 2
- [36] A. Seff, W. Zhou, N. Richardson, and R. P. Adams. Vitruvion: A generative model of parametric cad sketches. In *ICLR 2022 - 10th International Conference on Learning Representations*, 2022. Export Date: 07 July 2024; Cited By: 9. 3
- [37] H. Su, S. Maji, E. Kalogerakis, and E. Learned-Miller. Multi-view convolutional neural networks for 3d shape recognition. In *Proceedings of the IEEE International Conference on Computer Vision*, volume 2015 International Conference on Computer Vision, ICCV 2015, pages 945–953, 2015. Export Date: 31 July 2024; Cited By: 2865. 2
- [38] H. Thomas, C. R. Qi, J. E. Deschaut, B. Marcotegui, F. Goulette, and L. Guibas. Kpconv: Flexible and deformable convolution for point clouds. In *Proceedings of the IEEE International Conference on Computer Vision*, volume 2019-October, pages 6410–6419, 2019. Export Date: 31 July 2024; Cited By: 1705. 2
- [39] M. A. Uy, Y. Y. Chang, M. Sung, P. Goel, J. Lambourne, T. Birdal, and L. Guibas. Point2cyl: Reverse engineering 3d objects from point clouds to extrusion cylinders. In *Proceedings of the IEEE Computer Society Conference on Computer Vision and Pattern Recognition*, volume 2022-June, pages 11840–11850, 2022. Export Date: 23 July 2024; Cited By: 17. 2
- [40] P. S. Wang, Y. Liu, Y. X. Guo, C. Y. Sun, and X. Tong. Oct-cnn: Octree-based convolutional neural networks for 3d shape analysis. In *ACM Transactions on Graphics*, volume 36, 2017. Export Date: 31 July 2024; Cited By: 851. 2
- [41] Y. Wang, Y. Sun, Z. Liu, S. E. Sarma, M. M. Bronstein, and J. M. Solomon. Dynamic graph cnn for learning on point clouds. *ACM Transactions on Graphics*, 38(5), 2019. Export Date: 08 October 2024; Cited By: 3926. 2, 7, 8
- [42] X. Wei, R. Yu, and J. Sun. View-gcn: View-based graph convolutional network for 3d shape analysis. In *Proceedings of the IEEE Computer Society Conference on Computer Vision and Pattern Recognition*, pages 1847–1856, 2020. Export Date: 31 July 2024; Cited By: 197. 2
- [43] Karl D.D. Willis, Pradeep Kumar Jayaraman, Hang Chu, Yunsheng Tian, Yifei Li, Daniele Grandi, Aditya Sanghi, Linh Tran, Joseph G. Lambourne, Armando Solar-Lezama, and Wojciech Matusik. Joinable: Learning bottom-up assembly of parametric cad joints. In *2022 IEEE/CVF Conference on Computer Vision and Pattern Recognition (CVPR)*. IEEE, June 2022. 2
- [44] K. D. D. Willis, P. K. Jayaraman, J. G. Lambourne, H. Chu, and Y. Pu. Engineering sketch generation for computer-aided design. In *IEEE Computer Society Conference on Computer Vision and Pattern Recognition Workshops*, pages 2105–2114, 2021. Export Date: 07 July 2024; Cited By: 30. 3
- [45] R. Wu, C. Xiao, and C. Zheng. Deepcad: A deep generative network for computer-aided design models. In *Proceedings of the IEEE International Conference on Computer Vision*,

- pages 6752–6762, 2021. Export Date: 23 July 2024; Cited By: 47. [2](#)
- [46] W. Wu, Z. Qi, and L. Fuxin. Pointconv: Deep convolutional networks on 3d point clouds. In *Proceedings of the IEEE Computer Society Conference on Computer Vision and Pattern Recognition*, volume 2019-June, pages 9613–9622, 2019. Export Date: 09 October 2024; Cited By: 1264. [2](#), [7](#), [8](#)
- [47] Z. Wu, S. Song, A. Khosla, F. Yu, L. Zhang, X. Tang, and J. Xiao. 3d shapenets: A deep representation for volumetric shapes. In *Proceedings of the IEEE Computer Society Conference on Computer Vision and Pattern Recognition*, volume 07-12-June-2015, pages 1912–1920, 2015. Export Date: 31 July 2024; Cited By: 4378. [2](#)
- [48] T. Xiang, C. Zhang, Y. Song, J. Yu, and W. Cai. Walk in the cloud: Learning curves for point clouds shape analysis. In *Proceedings of the IEEE International Conference on Computer Vision*, pages 895–904, 2021. Export Date: 31 July 2024; Cited By: 130. [2](#)
- [49] M. Xu, R. Ding, H. Zhao, and X. Qi. Paconv: Position adaptive convolution with dynamic kernel assembling on point clouds. In *Proceedings of the IEEE Computer Society Conference on Computer Vision and Pattern Recognition*, pages 3172–3181, 2021. Export Date: 31 July 2024; Cited By: 272.
- [50] M. Xu, J. Zhang, Z. Zhou, M. Xu, X. Qi, and Y. Qiao. Learning geometry-disentangled representation for complementary understanding of 3d object point cloud. In *35th AAAI Conference on Artificial Intelligence, AAAI 2021*, volume 4A, pages 3056–3064, 2021. Export Date: 31 July 2024; Cited By: 58. [2](#)
- [51] X. Xu, K. D. D. Willis, J. G. Lambourne, C. Y. Cheng, P. K. Jayaraman, and Y. Furukawa. Skexgen: Autoregressive generation of cad construction sequences with disentangled codebooks. In *Proceedings of Machine Learning Research*, volume 162, pages 24698–24724, 2022. Export Date: 23 July 2024; Cited By: 15. [3](#)
- [52] Y. Xu, T. Fan, M. Xu, L. Zeng, and Y. Qiao. Spidercnn: Deep learning on point sets with parameterized convolutional filters. In *Lecture Notes in Computer Science (including sub-series Lecture Notes in Artificial Intelligence and Lecture Notes in Bioinformatics)*, volume 11212 LNCS, pages 90–105, 2018. Export Date: 08 October 2024; Cited By: 139. [2](#), [8](#)
- [53] Z. Yang and L. Wang. Learning relationships for multi-view 3d object recognition. In *Proceedings of the IEEE International Conference on Computer Vision*, volume 2019-October, pages 7504–7513, 2019. Export Date: 31 July 2024; Cited By: 125. [2](#)
- [54] T. Yu, J. Meng, and J. Yuan. Multi-view harmonized bilinear network for 3d object recognition. In *Proceedings of the IEEE Computer Society Conference on Computer Vision and Pattern Recognition*, pages 186–194, 2018. Export Date: 31 July 2024; Cited By: 240. [2](#)
- [55] Z. Zhang, B. S. Hua, and S. K. Yeung. Shellnet: Efficient point cloud convolutional neural networks using concentric shells statistics. In *Proceedings of the IEEE International Conference on Computer Vision*, volume 2019-October, pages 1607–1616, 2019. Export Date: 31 July 2024; Cited By: 313. [2](#)
- [56] H. Zhao, L. Jiang, J. Jia, P. Torr, and V. Koltun. Point transformer. In *Proceedings of the IEEE International Conference on Computer Vision*, pages 16239–16248, 2021. Export Date: 31 July 2024; Cited By: 927. [2](#)
- [57] S. Zhou, T. Tang, and B. Zhou. Cadparser: A learning approach of sequence modeling for b-rep cad. In *IJCAI International Joint Conference on Artificial Intelligence*, volume 2023-August, pages 1804–1812, 2023. Export Date: 23 July 2024; Cited By: 0. [2](#)